Applied Physics Letters

Precessed electron diffraction study of defects and strain in GaN nanowires fabricated by top-down etching

Cite as: Appl. Phys. Lett. **121**, 082104 (2022); https://doi.org/10.1063/5.0101908
Submitted: 04 June 2022 • Accepted: 30 July 2022 • Published Online: 23 August 2022

Gemma Martín, Lluís López-Conesa, Daniel del Pozo, et al.

COLLECTIONS

EP This paper was selected as an Editor's Pick

ARTICLES YOU MAY BE INTERESTED IN

Precessed electron diffraction study of defects and strain in GaN nanowires fabricated by top-down etching

Cite as: Appl. Phys. Lett. **121**, 082104 (2022); doi: 10.1063/5.0101908
Submitted: 4 June 2022 · Accepted: 30 July 2022 ·
Published Online: 23 August 2022

View Online Export Citation CrossMark

Gemma Martín,[1,2,3,a)] Lluís López-Conesa,[1,2,3] Daniel del Pozo,[2] Quim Portillo,[4] George Doundoulakis,[5,6] Alexandros Georgakilas,[5,6] Sònia Estradé,[1,2] and Francesca Peiró[1,2]

AFFILIATIONS

[1]LENS/MIND, Department of Electronics and Biomedical Engineering, Universitat de Barcelona, C/Martí i Franquès 1, 08028 Barcelona, Spain
[2]Institute of Nanoscience and Nanotechnology (IN2UB), Universitat de Barcelona, C/Martí i Franquès 1, 08028 Barcelona, Spain
[3]Centres Científics i Tecnològics de la Universitat de Barcelona. Solé i Sabaris, 1-3, 08028 Barcelona, Spain
[4]NanoMEGAS SPRL, Blvd Edmond Machtens 79, B-1080 Brussels, Belgium
[5]Microelectronics Research Group (MRG), IESL, FORTH, P.O. Box 1385, 71110 Heraklion, Greece
[6]Department of Physics, University of Crete, 71203 Heraklion, Greece

[a)]Author to whom correspondence should be addressed: gemmamartin@ub.edu

ABSTRACT

Gallium nitride (GaN) nanowires (NWs) have been fabricated by top-down etching from GaN heteroepitaxial films, which provides an accurate control of their position and dimensions. However, these NWs contain, similar to the initial GaN films, high density of structural defects such as threading dislocations (TDs). In this work, different strategies to reduce the density of defects along the NWs have been compared based on two different wet etching approaches followed by a rapid thermal annealing (RTA) at 750 °C. The addition of a 30 nm SiN_x coating is also explored. The defects and strain/stress along the NWs have been studied by high resolution transmission electron microscopy, diffraction contrast imaging in two-beam conditions and 4D STEM, as well as strain maps calculated from scanning precession electron diffraction measurements. RTA reduced the density of TDs at the middle of GaN NWs with bare surfaces by approximately 25%. The reduction increased to approximately 70% by RTA of GaN NWs with surfaces coated by amorphous SiN_x, which is attributed to enhancement of dislocation movements by stresses induced from differential thermal expansion of GaN and SiN_x. These results suggest a process route that, if optimized and combined with reduction of NW diameter, could establish etching as an efficient fabrication method for high crystal quality GaN NWs.

III–V semiconductors have been extensively explored as active materials for high-speed electronic devices and many types of optoelectronic and high-efficiency photovoltaic devices.[1,2] In particular, semiconductor nanowires (NWs) are of great interest due to their potential to reduce electronic and optical device length scales and their superior properties in comparison with heteroepitaxial films.[3–5] Among them, gallium nitride (GaN) nanowires have attracted much attention because of their unique material properties, such as wide direct bandgap, high saturation velocity, and large breakdown field.[6–11]

The fabrication of regular patterns of GaN vertical NWs requires an accurate control of position and dimensions, quite difficult to be achieved by spontaneous or selective seeded growth methods. The so-called bottom-up synthesis methods include plasma enhanced chemical vapor deposition,[12] metal–organic chemical vapor deposition,[13] laser-assisted catalytic growth,[14] and molecular beam epitaxy.[15,16] However, GaN nanowires can also be fabricated by a top-down approach.[17–19] This strategy offers advantages both in terms of the possibilities of dimension and aspect/ratio tuning and in view of their integration into existing large-scale fabrication platforms in micro and nanoelectronics devices. The main techniques for the top-down fabrication of anisotropic III–V nanostructures are plasma-based dry etches. However, these alone are not good enough for the obtention of both high quality and high aspect ratio III-nitride nanowires. The presence of threading dislocations (TDs) in top-down formed GaN NWs is probably the main disadvantage of the top-down method compared to spontaneously grown (bottom-up) defect free GaN NWs. Nevertheless, it may also be possible, using a proper thermal treatment or specific patterning, for TDs to fully "escape" (by glide or climb) from the lateral NW sides due to their limited diameter.[20] The movement of dislocations could be triggered by any stresses and it would be assisted by enhanced atomic diffusion at higher temperatures (e.g., annealing treatments).

The presence of defects and threading dislocations in GaN nanowires has been extensively studied for bottom-up fabrication procedures, being transmission electron microscopy one of the key tools to monitor the NW quality. However, TEM studies on GaN nanowires fabricated by top-down methods are scarce.

Among the different observation modes in a TEM, beam precession assisted electron diffraction (PED) in scanning mode is a very useful technique to unveil defects and strain distributions, since these 4D STEM datasets allow obtaining maps of the changes in the crystalline structure across very wide regions of the objects under study. The general term 4D STEM refers to a set of TEM techniques for which the scanning of a (convergent) electron beam over the specimen results in a four-dimensional dataset.[21] Although spectroscopic tomographic experiments also result in 4D datasets,[22–24] the term 4D STEM usually refers to spatially localized electron diffraction data: for each probe position (2D in real space), a diffraction pattern is acquired (2D in reciprocal space). A large amount of information is available from such datasets. Virtual bright field (BF) or dark field (DF) images can be generated by placing virtual detectors, i.e., selecting the appropriate regions of the reciprocal space with different mask geometries (circular, annular, etc.).[25] Differential phase contrast images can be obtained by mapping the direct beam deflection due to electric/magnetic fields in the specimen.[26–28] The analysis of the diffraction spot position and intensities can be used to obtain crystal phase, orientation,[29] and strain maps[30] over the scanned region.

For this last set of applications, usually grouped under the name of nanobeam electron diffraction, results can be greatly improved by the use of beam precession. By precessing the electron beam over the specimen on a hollow cone geometry,[31] the intersection of the Ewald sphere of electron k-moment and the reciprocal space of the sample integrate over a range of excitation errors, reducing the overall effect of dynamical scattering and resulting in (i) more spots in the diffraction pattern and (ii) more accurate intensities for their indexation. Figure S1 of the supplementary material shows a schematic of a scanning precession electron diffraction experiment, with the precession of the beam above the specimen and the subsequent descan of the direct and diffracted beams under the specimen.

In this work, we apply 4D STEM techniques to investigate the structural properties of GaN NWs fabricated by a top-down approach using two different wet chemical etching treatments based on a tetramethylammonium hydroxide (TMAH) and potassium hydroxide (KOH) solutions.[17,18,32] A rapid thermal annealing (RTA) at 750 °C, which is commonly used for Ohmic contacts in GaN films,[17] was also applied as a possible way to enhance the movement of threading dislocations. Finally, the effect of a 30 nm SiN_x deposition, which could act as the MIS dielectric in a MISFET vertical GaN NW transistor, is studied.

The epitaxial GaN structure was grown on a sapphire (0001) substrate by plasma assisted molecular beam epitaxy (PAMBE),[33] consisting (from top to bottom) of 1500-nm-thick non-intentionally doped GaN with electron concentration of approximately 10^{16} cm^{-3} and 30-nm thick AlN layer. This structure was cut into pieces and each piece was processed to obtain vertical GaN nanowires (NWs) following three conventional nanofabrication steps: (1) electron-beam lithography, (2) reactive-ion etching (RIE), and (3) anisotropic wet-chemical etching based on a tetramethylammonium hydroxide (TMAH) or potassium hydroxide (KOH) solution.[17,18,32] Details about the top-down formation of GaN NWs can be found elsewhere.[17]

Four vertical GaN NWs samples with a nominal diameter of 200 nm and height and pitch (distance between adjacent columns) of 1 μm have been fabricated using this top-down approach on the described epitaxial GaN-based structure. Therefore, although the first steps of the fabrication were the same for all samples, two different wet etching approaches (30 min in a TMAH-based solution or 30 min in a KOH-based solution) were used in order to investigate their influence on the structural properties of the resulting GaN NWs. Moreover, the effect of 2-min RTA at 750 °C chemical etching was also examined. Figure 1(a) illustrates that RIE formed trapezoidal GaN device nanostructures with nominal diameters of 220–700 nm from top to bottom. Figure 1(b) shows the final fabricated GaN NW array with a fixed nominal diameter of 200 nm and height and pitch of 1 μm, after RIE and anisotropic wet chemical etching in a TMAH-based developer. An identical picture is observed in the case of the KOH-based wet chemical treatment.

TEM thin lamellas were prepared precisely at the nanowires (see Fig. S2 of the supplementary material) by focused ion beam (FIB, Helios Nanolab 650, FEI, operated at 30 kV) using the lift-out technique.[34,35] An in-depth analysis based on high resolution transmission electron microscopy (HRTEM) and scanning TEM (STEM) imaging was carried out in a Jeol 2010F TEM operated at 200 kV coupled with a GIF Gatan filter. Chemical analysis was performed with the same instrument in the STEM mode by electron energy loss spectroscopy (EELS).[36,37]

Electron diffraction datasets in the scanning mode using electron beam precession were acquired employing a NanoMEGAS's "DigiSTAR" add-on device. In these experiments, a small precessed beam is scanned across the specimen and a (nano)diffraction pattern is acquired for every pixel synchronously with the scan. Strain analysis was carried out using the TopSpin software. In the processing, the intensity of the direct beam is used to generate a virtual bright field image and the positions of the diffraction spots are analyzed in order to find possible distortions in distances and/or angles from a region defined as an unstrained reference. These positions are used to calculate the strain tensor (ε) in order to obtain strain maps in the specimen.

First, dimensions and composition of the GaN nanowires were assessed by TEM. GaN nanowires have diameters of 200 nm and heights and distances between them of 1 μm [see Fig. 2(a)], in agreement with nominal values. Neither the diameter nor the height of the nanowires has a significant dependence on the type of wet etching or the application of RTA processes.

HRTEM images [Fig. 2(b)] and corresponding FFTs show the hexagonal wurtzite crystalline structure for GaN nanowires with smooth vertical sidewalls. Moreover, as can be seen in Fig. 2(c), very

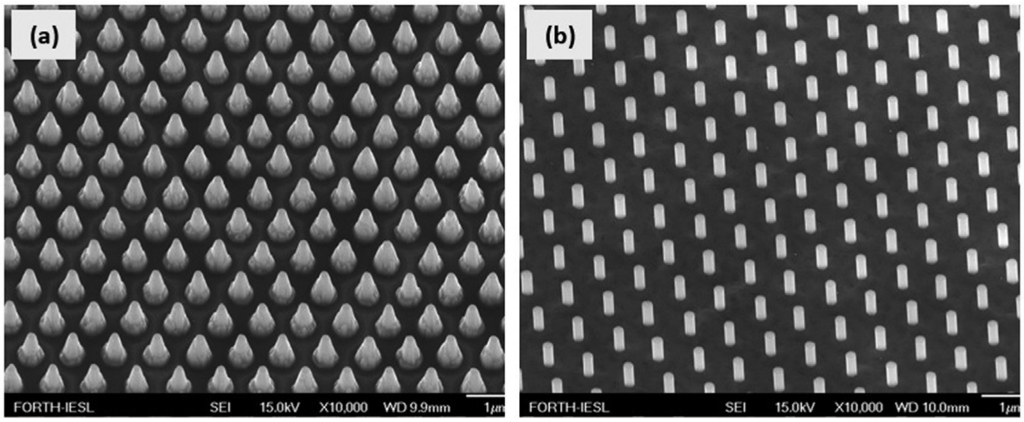

FIG. 1. SEM images in tilted-view of (a) a trapezoidal GaN NW array after RIE of the GaN film and (b) the final GaN NW array after RIE and anisotropic wet chemical etching in a TMAH-based developer.

few threading dislocations have been observed in all the cases. Thus, in order to perform an in-depth study of the presence of defects and dislocations along the GaN nanowires, two-beam condition diffraction contrast imaging mode has been used.

Figure 3 shows bright field images under two-beam condition using g parallel to the [0001] direction of different GaN nanowires fabricated by (a) WE1 (TMAH) without RTA, (b) WE2 (KOH) without RTA, (c) WE1 with RTA, and (d) WE2 with RTA process at 750 °C.

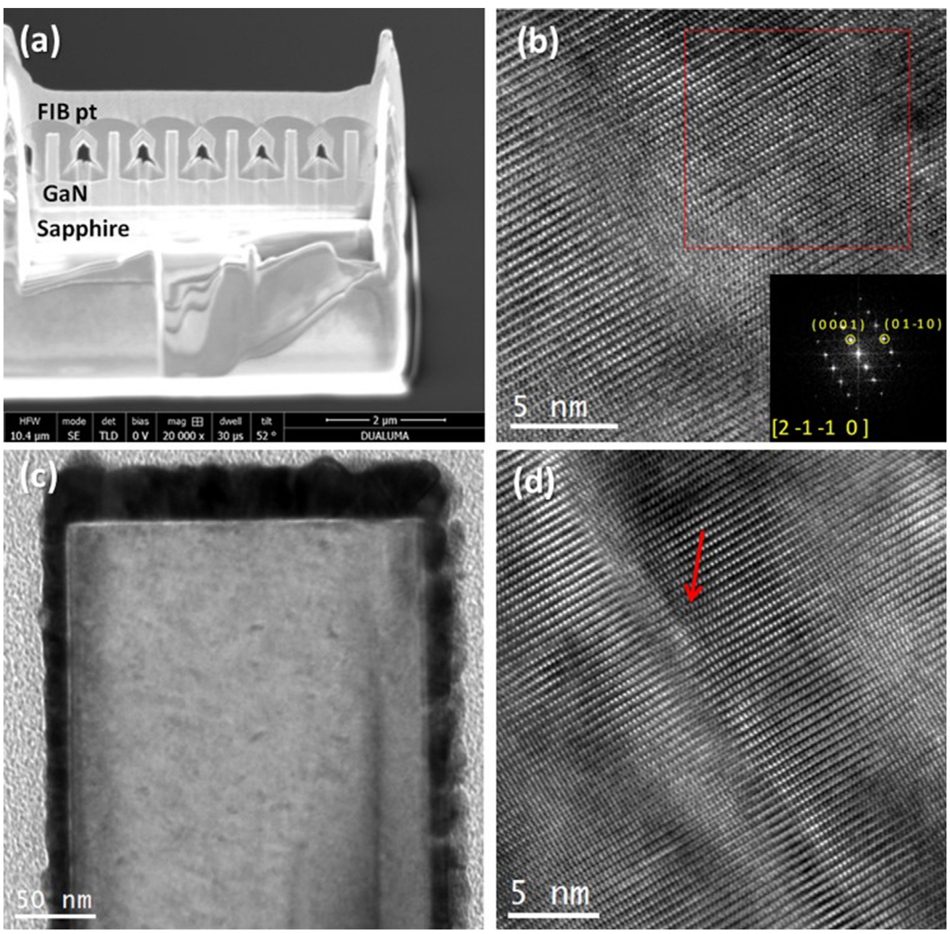

FIG. 2. (a) SEM image of the TEM lamella preparation of GaN nanowires, (b) HRTEM image of the GaN nanowire and its corresponding FFT as inset, (c) TEM image of a GaN nanowire showing the presence of very few threading dislocations, and (d) HRTEM image containing the threading dislocation present in the GaN nanowire.

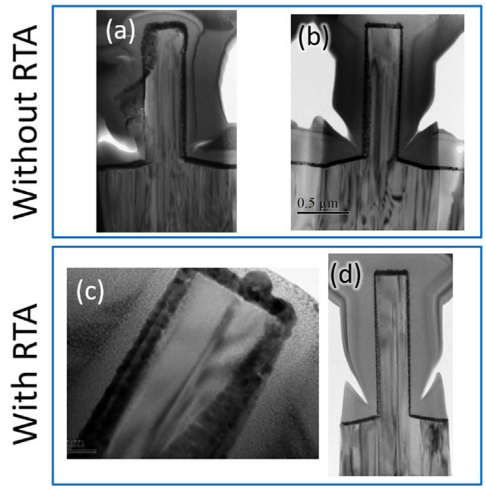

FIG. 3. Bright field images under two-beam condition using reflections along [0001] of the different GaN nanowires fabricated by using (a) WE1 without RTA, (b) WE2 without RTA, (c) WE1 with RTA, and (d) WE2 with RTA.

As can be seen in Fig. 3, the density of threading dislocations is reduced after RTA. In this sense, the threading dislocation density (TDD) has been estimated as an average, counting the number of threading dislocations found through an imaginary line perpendicular to the growth direction at the middle and the top of the nanowire, measuring several nanowires for the different fabrication conditions. The results are summarized in Table I. Thus, the TDD is reduced to 66% (from 1.2×10^5 to 0.4×10^5 dislocations/cm) at the top and to 25% (from 1.6×10^5 to 1.2×10^5 dislocations/cm) at the middle of the nanowire for WE1 samples and to 29% (from 0.7×10^5 to 0.5×10^5 dislocations/cm) at the top and to 23% (from 1.3×10^5 to 1.0×10^5 dislocations/cm) at the middle of the nanowire for WE2 samples after annealing.

The reduced TDD of the samples after the RTA annealing is mainly attributed to movement of dislocations assisted by enhanced atomic diffusion at higher temperatures. Moreover, the sample with the TMAH treatment exhibited reduced TDD at the top of GaN NWs compared with that with the KOH treatment. The origin of this observation is not clearly understood and may be related to different chemical reactions that take place during these two chemical treatments. However, further experimental and theoretical studies are needed for a comprehensive conclusion, which are beyond the scope of this study. It should be noticed though that after RTA both samples exhibited a rather similar TDD at the top and middle of NWs, which suggests that RTA is an efficient treatment for improving the structure of etched NWs.

TABLE I. Density of threading dislocations (in 10^5 dislocations/cm) for the different synthesis routes, measured at the top and the middle of the NWs.

	No RTA		RTA	
	Top	Middle	Top	Middle
WE1 (TMAH)	1.2	1.6	0.4	1.2
WE2 (KOH)	0.7	1.3	0.5	1.0
WE1 + SiN_x			0.3	0.5

Until now, conventional TEM has been used to demonstrate the suitability of top-down fabrication techniques to control the dimension and position of GaN nanowires, and the effect of RTA treatments after the etching to control the TDD along the nanowires. Moreover, electron diffraction can be used to determine the crystalline structure of the nanowires. In this case, the measured values for the a and c values of the wurtzite structure were 3.2 and 5.1 Å, respectively, as expected for bulk GaN. Nevertheless, the information obtained from SAED patterns comes from extended regions of the nanowire and consequently, defects or local variations are not detectable. In order to study local parameters of the crystalline structure and relative variations through the nanowire, we have used an innovative technique to perform an in-depth study of the strain distribution along the GaN nanowires: 4D STEM strain mapping using precession electron diffraction (PED) in the scanning mode.

The GaN NWs were systematically studied by mapping the strain in rectangular regions with a height of 100 nm located at the center of the GaN nanowire, at 10 nm from the top. Figure 4 shows these maps for the GaN NW after the two different etching methods and after the subsequent RTA annealing. The growth direction of the nanowires is defined as y, as indicated by the arrow on the nanodiffraction pattern in Fig. S4 of the supplementary material, and the perpendicular is defined as x. The strain maps of the GaN nanowires fabricated without the RTA process show abrupt changes in the strain state in the x direction, probably due to the presence of threading dislocations.

Additional strain maps obtained in the lower region of the NWs are included in the supplementary material (Fig. S3).

For the nanowires submitted to the RTA treatment, the strain maps are more homogeneous, although local strained regions (highlighted with red circles in Fig. 4) remain in both ε_{xx} and ε_{yy} components in the WE2 case. The tensile strain measured in x-direction

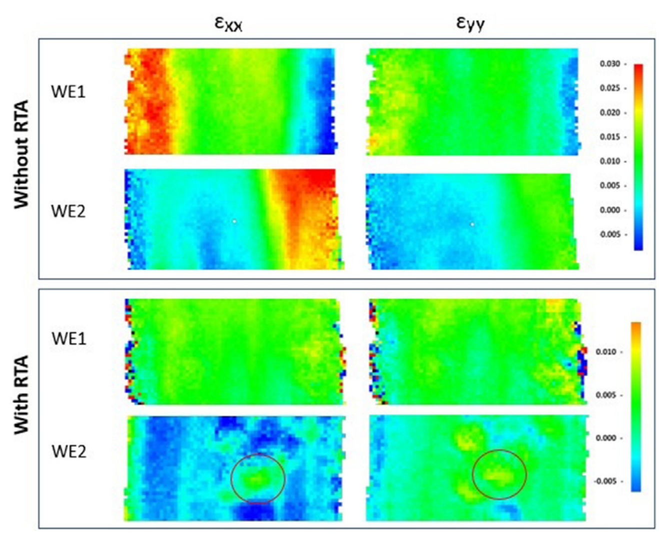

FIG. 4. Strain maps along the x and y directions for untreated and RTA treated GaN NWs fabricated using WE1 and WE2. Note the change in the strain color scale, showing lower strain values for the RTA treated NWs.

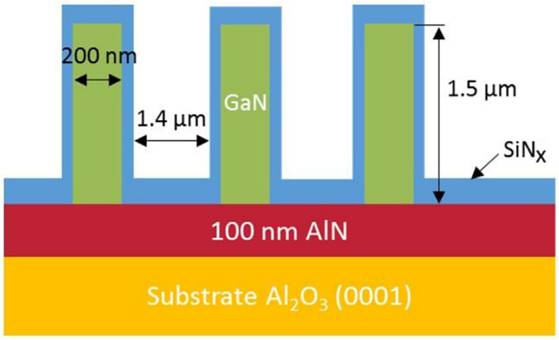

FIG. 5. Schematic showing the cross-sectional view of the sample consisting of GaN NWs covered by SiN_x with a nominal (planar) deposition thickness of 30 nm.

from the center to the edges (see Fig. 4) is up to 0.03% for nanowires fabricated without RTA process. The corresponding value in the case of nanowires fabricated with RTA process is less than 0.01%. This is in agreement with the reduction in the TDD after the RTA process, calculated from TEM images.

As SiN_x is usually used as a dielectric material, an additional GaN NW sample with a nominal diameter of 200 nm, a height of 1.5 μm, and a pitch of 1.4 μm, using the same top-down technique (TMAH treatment), with a final nominal/planar deposition of 30 nm SiN_x by plasma-enhanced chemical vapor deposition (PECVD) was also fabricated and characterized. The SiN_x deposition covered also the sidewalls of GaN NWs. A schematic showing the structure of the SiN_x/GaN heterostructure NWs is shown in Fig. 5.

First, conventional TEM was used to study dimensions, composition, and crystallinity. GaN nanowires with the SiN_x coating have a diameter of 200 nm, a height of 1.5 μm, and a distance between them of 1.4 μm (see Fig. 5), in agreement with the nominal values. Moreover, the SiN_x coating is amorphous with a thickness that ranges from 8 to 15 nm at the lateral side of the NW and from 20 to 35 nm at the top of the NW. Additionally, as can be seen in Fig. S5 of the supplementary material, EELS measurements confirmed the presence of Si and N at the coating, revealing also a higher concentration of Si in the outer part of the coating and lower concentration when approaching the GaN. The HRTEM observation of the sample assessed the good crystallinity of the GaN nanowire and the presence of threading dislocations along its growth direction. Moreover, the dislocation density in the GaN nanowires with the SiN_x coating is reduced by 75% (from 1.2×10^5 to 0.3×10^5 dislocations/cm) at the top and by 69% (from 1.6×10^5 to 0.5×10^5 dislocations/cm) in the middle of the nanowire compared with the GaN nanowires fabricated with the same TMAH treatment (see Table I). The dislocation density is also lower by 25% (0.3×10^5 vs 0.4×10^5 dislocations/cm) at the top and by 60% (0.5×10^5 vs 1.2×10^5 dislocations/cm) in the middle of the nanowire compared to the GaN nanowires fabricated with the TMAH treatment and subject to RTA treatment (see Table I).

Strain maps obtained for the GaN nanowire with the SiN_x coating are shown in Fig. 6. The tensile strain on the y axis (εyy) changes perpendicularly to the growth direction with values up to 0.5% from the center to the edges, indicative of a strain at the edges with respect to the reference at the central part of the NW. Moreover, the compressive strain in x axis (εxx) changes periodically along the growth direction near to the GaN/SiN_x interface in around 0.2%. Finally, Fig. 6 shows compressive strain, highlighted with a red circle, due to the presence of a local defect.

In summary, RTA treatment resulted in a decrease in the density of threading dislocations in the GaN NWs, for both TMAH and KOH etching, as evidenced from diffraction contrast imaging, through direct counting, and from PED strain mapping in the form of a more homogeneous strain distribution. In this fabrication route, threading dislocations that are present in the heteroepitaxial GaN films may also remain in the etched GaN NWs. However, it may be possible for them to fully escape from the lateral nanowire sides due to the limited diameter of NWs. The movement of dislocations could be triggered by any stresses and it would be assisted by enhanced atomic diffusion at higher temperatures (e.g., RTA treatments).

The RTA treatment exhibited a stronger dislocation density reduction effect when applied on the SiN_x covered GaN NWs and significant tensile strain values in the c-axis (εNW) of these NWs were

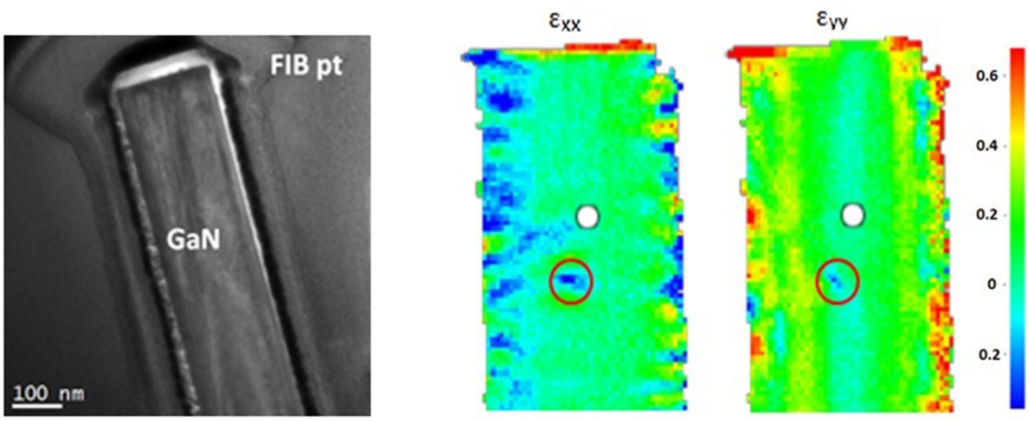

FIG. 6. Bright field image of the GaN NW (fabricated with TMAH treatment) covered with a SiN_x layer and then subject to RTA at 750 °C. Strain maps for the x axis (εxx) and y axis (εyy), perpendicular and parallel to the growth direction, respectively. An increase in tensile strain on the y axis (εyy) is observed from the center of the NW, defined as a reference, toward the edges. Periodic regions of compressive strain on the x axis (εxx) are observed along the growth direction at the GaN/SiN_x interface. Smaller strain features probably from point defects are also detected.

observed. This is attributed to the creation of thermal stresses in the GaN NW crystal, during RTA temperature cycling, due to its contact (interface) with the SiN_x coating layer and the different thermal expansion coefficients (TECs) of GaN and SiN_x. The exact values of TECs might be questionable, but certainly, GaN[38] exhibits significantly higher TECs along both its c and a axes compared to Si_3N_4.[39] The SiN_x/GaN hetero-interface area extends mainly on the lateral faces of the 1.5 μm high nanowires. Anticipating a significant strain relaxation at the maximum temperature of RTA (750 °C), the cooling of the sample would create, along the nanowire axis, tensile strain in the GaN crystal (as observed in Fig. 6) and compressive strain in the SiN_x layer. Overall, the formation of a nanowire heterostructure could enable the creation of thermal stresses by temperature cycling, which could effectively move dislocations out of the NW crystal. A significantly stronger effect is expected by reducing the NW diameter, compared to the 200 nm of this study.

This work also indicates that conventional device nanofabrication techniques, such as Ohmic contact annealing and deposition of MIS dielectric, could reduce the threading dislocation density of the top-down GaN NW structures and enhance their device characteristics. These results are promising and further optimization of these techniques may result to defect-free NWs with structural characteristics comparable with the bottom-up ones.

In conclusion, the microstructure of top-down fabricated GaN nanowires has been studied using TEM imaging and diffraction techniques. The effect of two different wet etching processes and a rapid thermal annealing step on this microstructure has been assessed. From diffraction contrast imaging, a decrease in the density of threading dislocations after RTA has been found. This agrees with the strain maps, obtained using precessed electron diffraction, which show a more homogeneous and reduced strain state across the NWs, after the RTA process. The RTA effect was maximized on GaN NWs covered by SiN_x dielectric, thus forming SiN_x/GaN heterostructure NWs. 4D STEM, and in particular, strain mapping by scanning PED, has demonstrated its potential for the characterization of this kind of nanostructures. Compared to other available strain mapping techniques, it offers a large area of mapping (vs geometric phase analysis[40]) and a rather simple experimental setup (vs dark field electron holography[41]).

See the supplementary material for an schematic that shows precession of the scanned electron beam over the specimen in a hollow cone geometry; an image with the steps in the preparation of the TEM specimen using the FIB lift-out technique; the strain maps along the x and y directions from the lower regions of the NWs for the untreated and RTA treated GaN NWs; and an example of a spatially localized precessed electron nanodiffraction pattern and EELS map from the SiN_x coated GaN NW.

The research leading to these results received funding from the Spanish Ministry of Science and Innovation (Nos. PID2019-106165GB-C21, RED2018-102609-T, and RTI2018-094291-B-I00) and the Catalan Government (No. 2017 SGR776). We also acknowledge the TEM facilities at the Technological and Scientific Centers of the University of Barcelona (CCiT-UB) and FIB facilities at Centro de Bioinnovación of the University of Malaga (UMA). The work in Greece has been supported by the Hellenic Foundation for Research and Innovation (HFRI) (Project: EPINEET and Grant No. HFRI-FM17-3173).

AUTHOR DECLARATIONS

Conflict of Interest

The authors have no conflicts to disclose.

Author Contributions

Gemma Martin: Formal analysis (equal); Investigation (equal); Methodology (equal); Validation (equal); Writing – original draft (equal); Writing – review and editing (equal). **Lluís López-Conesa:** Formal analysis (equal); Investigation (equal); Methodology (equal); Validation (equal); Writing – original draft (equal); Writing – review and editing (equal). **Daniel del Pozo:** Formal analysis (equal); Writing – review and editing (equal). **Quim Portillo:** Conceptualization (equal); Methodology (equal); Resources (equal). **George Doundoulakis:** Formal analysis (equal); Investigation (equal); Validation (equal); Writing – review and editing (equal). **Alexandros Georgakilas:** Formal analysis (equal); Validation (equal); Writing – review and editing (equal). **Sonia Estrade:** Formal analysis (equal); Methodology (equal); Supervision (equal); Validation (equal); Writing – original draft (equal); Writing – review and editing (equal). **Francesca Peiró:** Formal analysis (equal); Funding acquisition (equal); Methodology (equal); Project administration (equal); Resources (equal); Supervision (equal); Validation (equal); Writing – original draft (equal); Writing – review and editing (equal).

DATA AVAILABILITY

The data that support the findings of this study are available from the corresponding author upon reasonable request.

REFERENCES

[1] A. Y. Polyakov, T. Kim, I. H. Lee, and S. J. Pearton, "III-nitride nanowires as building blocks for advanced light emitting diodes," Phys. Status Solidi B **256**, 1800589 (2019).

[2] S. C. Jain, M. Willander, J. Narayan, and R. Van Overstraeten, "III-nitrides: Growth, characterization, and properties," J. Appl. Phys. **87**, 965–1006 (2000).

[3] J. Sun, M. Han, Y. Gu, Z. Yang, and H. Zeng, "Recent advances in group III-V nanowire infrared detectors," Adv. Opt. Mater. **6**, 1800256 (2018).

[4] R. R. Lapierre, M. Robson, K. M. Azizur-Rahman, and P. Kuyanov, "A review of III-V nanowire infrared photodetectors and sensors," J. Phys. D **50**, 123001 (2017).

[5] Z. Li, H. H. Tan, C. Jagadish, and L. Fu, "III-V semiconductor single nanowire solar cells: A review," Adv. Mater. Technol. **3**, 1800005 (2018).

[6] S. Mariana, J. Gülink, G. Hamdana, F. Yu, K. Strempel, H. Spende, N. Yulianto, T. Granz, J. D. Prades, E. Peiner, H. S. Wasisto, and A. Waag, "Vertical GaN nanowires and nanoscale light-emitting-diode arrays for lighting and sensing applications," ACS Appl. Nano Mater. **2**, 4133–4142 (2019).

[7] M. Asif Khan, A. Bhattarai, J. N. Kuznia, and D. T. Olson, "High electron mobility transistor based on a GaN-$Al_xGa_{1-x}N$ heterojunction," Appl. Phys. Lett. **63**, 1214–1215 (1993).

[8] B. S. Eller, J. Yang, and R. J. Nemanich, "Electronic surface and dielectric interface states on GaN and AlGaN," J. Vac. Sci. Technol. A **31**, 050807 (2013).

[9] J. A. Del Alamo and E. S. Lee, "Stability and reliability of lateral GaN power field-effect transistors," IEEE Trans. Electron Devices **66**, 4578–4590 (2019).

[10] M. Hugues, P. A. Shields, F. Sacconi, M. Mexis, M. Auf Der Maur, M. Cooke, M. Dineen, A. Di Carlo, D. W. E. Allsopp, and J. Zúñiga-Pérez, "Strain evolution in GaN nanowires: From free-surface objects to coalesced templates," J. Appl. Phys. **114**, 084307 (2013).

[11]H. Stanchu, V. Kladko, A. V. Kuchuk, N. Safriuk, A. Belyaev, A. Wierzbicka, M. Sobanska, K. Klosek, and Z. R. Zytkiewicz, "High-resolution x-ray diffraction analysis of strain distribution in GaN nanowires on Si(111) substrate," Nanoscale Res. Lett. **10**, 51 (2015).
[12]J. W. Zhao, Y. F. Zhang, Y. H. Li, C. H. Su, X. M. Song, H. Yan, and R. Z. Wang, "A low cost, green method to synthesize GaN nanowires," Sci. Rep. **5**, 17692 (2015).
[13]T. Kuykendall, P. Pauzauskie, S. Lee, Y. Zhang, J. Goldberger, and P. Yang, "Metalorganic chemical vapor deposition route to GaN nanowires with triangular cross sections," Nano Lett. **3**, 1063–1066 (2003).
[14]X. Duan and C. M. Lieber, "Laser-assisted catalytic growth of single crystal GaN nanowires," J. Am. Chem. Soc. **122**, 188–189 (2000).
[15]S. Eftychis, J. Kruse, T. Koukoula, T. Kehagias, P. Komninou, A. Adikimenakis, K. Tsagaraki, M. Androulidaki, P. Tzanetakis, E. Iliopoulos, and A. Georgakilas, "Understanding the effects of Si(111) nitridation on the spontaneous growth and properties of GaN nanowires," J. Cryst. Growth **442**, 8–13 (2016).
[16]K. A. Bertness, A. Roshko, L. M. Mansfield, T. E. Harvey, and N. A. Sanford, "Mechanism for spontaneous growth of GaN nanowires with molecular beam epitaxy," J. Cryst. Growth **310**, 3154–3158 (2008).
[17]G. Doundoulakis, A. Adikimenakis, A. Stavrinidis, K. Tsagaraki, M. Androulidaki, F. Iacovella, G. Deligeorgis, G. Konstantinidis, and A. Georgakilas, "Nanofabrication of normally-off GaN vertical nanowire MESFETs," Nanotechnology **30**, 285304 (2019).
[18]F. Yu, D. Rümmler, J. Hartmann, L. Caccamo, T. Schimpke, M. Strassburg, A. E. Gad, A. Bakin, H. H. Wehmann, B. Witzigmann, H. S. Wasisto, and A. Waag, "Vertical architecture for enhancement mode power transistors based on GaN nanowires," Appl. Phys. Lett. **108**, 213503 (2016).
[19]Y. W. Jo, D. H. Son, C. H. Won, K. S. Im, J. H. Seo, I. M. Kang, and J. H. Lee, "AlGaN/GaN FinFET with extremely broad transconductance by side-wall wet etch," IEEE Electron Device Lett. **36**, 1008–1010 (2015).
[20]M. Conroy, H. Li, V. Z. Zubialevich, G. Kusch, M. Schmidt, T. Collins, C. Glynn, R. W. Martin, C. O'Dwyer, M. D. Morris, J. D. Holmes, and P. J. Parbrook, "Self-healing thermal annealing: Surface morphological restructuring control of GaN Nanorods," Cryst. Growth Des. **16**, 6769–6775 (2016).
[21]C. Ophus, "Four-dimensional scanning transmission electron microscopy (4D-STEM): From scanning nanodiffraction to ptychography and beyond," Microsc. Microanal. **25**, 563–582 (2019).
[22]K. Jarausch, P. Thomas, D. N. Leonard, R. Twesten, and C. R. Booth, "Four-dimensional STEM-EELS: Enabling nano-scale chemical tomography," Ultramicroscopy **109**, 326–337 (2009).
[23]L. Yedra, A. Eljarrat, J. M. Rebled, L. López-Conesa, N. Dix, F. Sánchez, S. Estradé, and F. Peiró, "EELS tomography in multiferroic nanocomposites: From spectrum images to the spectrum volume," Nanoscale **6**, 6646–6650 (2014).
[24]P. Torruella, R. Arenal, F. de la Peña, Z. Saghi, L. Yedra, A. Eljarrat, L. López-Conesa, M. Estrader, A. López-Ortega, G. Salazar-Alvarez, J. Nogués, C. Ducati, P. A. Midgley, F. Peiró, and S. Estradé, "3D visualization of the iron oxidation state in FeO/Fe_3O_4 core–shell nanocubes from electron energy loss tomography," Nano Lett. **16**, 5068–5073 (2016).
[25]C. Gammer, V. Burak Ozdol, C. H. Liebscher, and A. M. Minor, "Diffraction contrast imaging using virtual apertures," Ultramicroscopy **155**, 1–10 (2015).
[26]N. J. Zaluzec, "Quantitative measurements of magnetic vortices using position resolved diffraction in lorentz STEM," in *Microscopy and Microanalysis* (Cambridge University Press, 2002), Vol. 8, pp. 376–377.
[27]M. W. Tate, P. Purohit, D. Chamberlain, K. X. Nguyen, R. Hovden, C. S. Chang, P. Deb, E. Turgut, J. T. Heron, D. G. Schlom, D. C. Ralph, G. D. Fuchs, K. S. Shanks, H. T. Philipp, D. A. Muller, and S. M. Gruner, "High dynamic range pixel array detector for scanning transmission electron microscopy," Microsc. Microanal. **22**, 237–249 (2016).
[28]J. A. Hachtel, J. C. Idrobo, and M. Chi, "Sub-Ångstrom electric field measurements on a universal detector in a scanning transmission electron microscope," Adv. Struct. Chem. Imaging **4**, 10 (2018).
[29]E. F. Rauch, J. Portillo, S. Nicolopoulos, D. Bultreys, S. Rouvimov, and P. Moeck, "Automated nanocrystal orientation and phase mapping in the transmission electron microscope on the basis of precession electron diffraction," Z. Kristallogr. **225**, 103–109 (2010).
[30]V. B. Ozdol, C. Gammer, X. G. Jin, P. Ercius, C. Ophus, J. Ciston, and A. M. Minor, "Strain mapping at nanometer resolution using advanced nano-beam electron diffraction," Appl. Phys. Lett. **106**, 253107 (2015).
[31]R. Vincent and P. a Midgley, "Double conical beam-rocking system for measurement of integrated electron diffraction intensities," Ultramicroscopy **53**, 271–282 (1994).
[32]Y. W. Jo, D. H. Son, D. G. Lee, C. H. Won, J. H. Seo, I. M. Kang, and J. H. Lee, "First demonstration of GaN-based vertical nanowire FET with top-down approach," in *Device Research Conference - Conference Digest, DRC 2015-August* (Institute of Electrical and Electronics Engineers Inc., 2015), pp. 35–36.
[33]A. Georgakilas, H. M. Ng, and P. Komninou, "Plasma-Assisted molecular beam epitaxy of III-V nitrides," in *Nitride Semiconductors* (Wiley-VCH Verlag GmbH & Co. KGaA, 2006), pp. 107–191.
[34]R. M. Langford and C. Clinton, "*In situ* lift-out using a FIB-SEM system," Micron **35**, 607–611 (2004).
[35]L. A. Giannuzzi and F. A. Stevie, "A review of focused ion beam milling techniques for TEM specimen preparation," Micron **30**, 197–204 (1999).
[36]D. B. Williams and C. B. Carter, "The transmission electron microscope," in *Transmission Electron Microscopy* (Springer US, 2009), pp. 3–22.
[37]R. F. Egerton, "An introduction to EELS," in *Electron Energy-Loss Spectroscopy in the Electron Microscope* (Springer US, 2011), pp. 1–28.
[38]C. Roder, S. Einfeldt, S. Figge, and D. Hommel, "Temperature dependence of the thermal expansion of GaN," Phys. Rev. B. **72**, 085218 (2005).
[39]T. M. Phung, D. C. Johnson, and G. A. Antonelli, "A detailed experimental and analytical study of the thermal expansion of dielectric thin films on Si by x-ray reflectivity," J. Appl. Phys. **100**, 064317 (2006).
[40]M. J. Hÿtch, E. Snoeck, and R. Kilaas, "Quantitative measurement of displacement and strain fields from HREM micrographs," Ultramicroscopy **74**, 131–146 (1998).
[41]A. Béché, J. L. Rouvière, J. P. Barnes, and D. Cooper, "Dark field electron holography for strain measurement," Ultramicroscopy **111**, 227–238 (2011).